JACS
JOURNAL OF THE AMERICAN CHEMICAL SOCIETY
Article
Cite This: J. Am. Chem. Soc. 2018, 140, 11085−11090
pubs.acs.org/JACS

$Cs_2PbI_2Cl_2$, All-Inorganic Two-Dimensional Ruddlesden−Popper Mixed Halide Perovskite with Optoelectronic Response

Jiangwei Li,[†,‡,∥] Qin Yu,[†,∥] Yihui He,[‡] Constantinos C. Stoumpos,[‡] Guangda Niu,[§] Giancarlo G. Trimarchi,[‡] Hang Guo,[†] Guifang Dong,[†] Dong Wang,*[,†] Liduo Wang,[†] and Mercouri G. Kanatzidis*[,‡]

[†]Department of Chemistry, Tsinghua University, Beijing 100084, China
[‡]Department of Chemistry, Northwestern University, Evanston, Illinois 60208, United States
[§]Wuhan National Laboratory for Optoelectronics and School of Optical and Electronic Information, Huazhong University of Science and Technology, Wuhan 430074, China

Supporting Information

ABSTRACT: The two-dimensional Ruddlesden−Popper (RP) phases are an important class of halide perovskites with versatile optoelectronic properties. So far, only organic−inorganic hybrid RP phases involving long organic spacers were reported in this class. Here, we report an all-inorganic RP phase lead halide perovskite, $Cs_2PbI_2Cl_2$ (**1**, $I4/mmm$ space group; a = 5.6385(8) Å, c = 18.879(4) Å), synthesized by a solid-state method. The compound exhibits a band gap of $E_g \sim 3.04$ eV and photoconductivity. We find an anomalous band gap evolution in $Cs_2Pb_{1-x}Sn_xI_2Cl_2$ solid solutions. Our combined density functional theory and experimental study supports the thermodynamically stable nature of **1** as a unique ordered phase in the Cs_2PbX_4 (X = Cl, Br, I) system. The calculations suggest that **1** is a direct bandgap semiconductor with relatively small effective carrier mass along the in-plane direction, consistent with the experimentally observed in-plane UV-light photoresponse. We also demonstrate that **1** is promising for radiation detection capable of α-particle counting. Moreover, **1** shows markedly ambient and thermal stability.

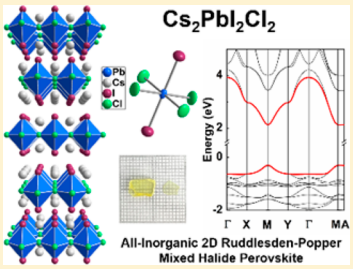

INTRODUCTION

Ruddlesden−Popper (RP) phases, with a general formula of $A_{n+1}B_nX_{3n+1}$ (n = 1, 2, ...), are one of the most common forms of layered perovskite structure, consisting of alternated two-dimensional (2D) perovskite slabs and spacer cations.[1] In the long investigated oxide perovskites (X = O^{2-}), many interesting properties have been demonstrated with RP structure, such as colossal magnetoresistance, superconductivity, ferroelectricity, orbital ordering transition, and catalytic activity.[2−6] Recently, the class of halide perovskites (B = Sn^{2+}, Pb^{2+}, X = Cl^-, Br^-, I^-) has been shown to exhibit unexpectedly excellent optoelectronic and photovoltaic properties, and 2D RP phases of lead halide perovskites have already been applied in high-efficiency solar cells and light-emitting diodes with higher stability.[7−10] However, all the reported 2D RP phase lead halide perovskites are hybrid organic−inorganic compounds with long organic chains, which are also known as ⟨100⟩-oriented 2D perovskites, and to the best of our knowledge, no record of all-inorganic RP phase halide perovskites has been reported.[9−16] Cs_2PbI_4 that corresponds to an all-inorganic RP phase with n = 1 was predicted to have a 1.5−1.9 eV band gap by theoretical calculations, which could be attractive for photovoltaic applications like tandem solar cell, however, to our knowledge, this compound does not exist.[17,18] Yu and co-workers claimed the plausible existence of RP phases in 2D $CsPbBr_3$ nanosheets, providing the possibility of stabilization effect in nanoscale.[19] In the case of "2D" $CsPbBr_3$, work on printed photodetectors with excellent photosensing and fast response times has been reported.[20] The purely inorganic RP phases of halide perovskites promise to exhibit a more robust nature relative to the hybrid organic−inorganic compounds under extreme conditions. Therefore, studying their physical and chemical properties is important. Here, we chose the largest inorganic spacer cation Cs^+ to support the perovskite framework and explored the basic chemistry of the Cs_2PbX_4 (X = Cl, Br, I) system. We report the new semiconducting RP compound $Cs_2PbI_2Cl_2$ with n = 1, formed by corner-sharing of elongated $[PbI_2Cl_4]$ octahedral units.

RESULTS AND DISCUSSION

The investigation in the Cs_2PbX_4 (X = Cl, Br, I) system was performed using solid-state synthesis, and the powder XRD results of the products are shown in Figure S2. When the binary starting materials with the same halide were used (e.g., 2CsX + PbX_2), the reaction products were composed of mixtures of $CsPbX_3$ ("113") and Cs_4PbX_6 ("416"). For reactions with different halide binary reactants (e.g., 2CsX + PbY_2, X ≠ Y), the results varied. When the halides were immediate neighbors in the periodic table for example in the 2CsBr + $PbCl_2$ and 2CsBr + PbI_2 cases, the products of "113"

Received: June 8, 2018
Published: August 7, 2018

DOI: 10.1021/jacs.8b06046
J. Am. Chem. Soc. 2018, 140, 11085−11090

and "416" phases we observed were in the form of mixed-halide solid solution (e.g., $CsPbBr_{3-x}Cl_x$, $Cs_4PbBr_{6-x}Cl_x$). When the halides were distant neighbors in the case of 2CsCl + PbI_2, we observed a new XRD pattern corresponding to the quaternary phase of $Cs_2PbI_2Cl_2$ with ordered I/Cl halides in the structure.

The structure of $Cs_2PbI_2Cl_2$ was solved and refined using single crystal X-ray crystallography (see SI file for details). As shown in Figure 1, $Cs_2PbI_2Cl_2$ adopts the K_2NiF_4-type

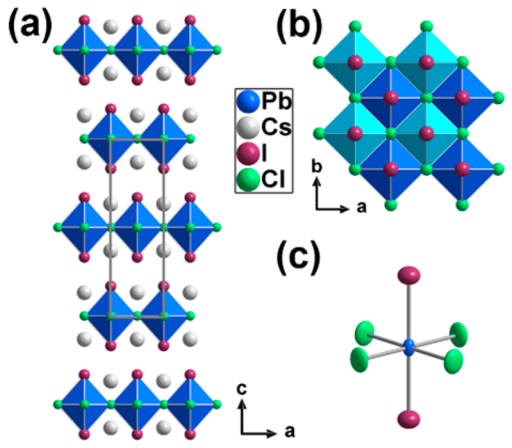

Figure 1. Crystal structure of $Cs_2PbI_2Cl_2$ from (a) the side view (unit cell outlined in gray) and (b) top-down view (Cs^+ are hidden and the adjacent perovskite slabs are in different color to depict the relative stacking of layers with (1/2, 1/2) displacement), and (c) the elongated $[PbI_2Cl_4]$ octahedral unit. Selective bond length: Pb–Cl (2.8193(4) Å), Pb–I (3.171(2) Å), and Cs–I (3.781(3) Å).

structure[1] and crystallizes in the tetragonal space group of $I4/mmm$ (no. 139) with the unit cell parameters of $a = b = 5.6385(8)$ Å, $c = 18.879(4)$ Å. The 2D $[PbI_2Cl_2]_n^{2n-}$ plane is constructed by the corner-sharing Pb-centered $[PbI_2Cl_4]^{4-}$ unit, where Cl ions occupy in-plane sites serving as the shared corners of the Pb octahedron and I ions occupy out-of-plane halide sites serving as terminal ligands. With the Cs^+ spacer ions balancing charge, $Cs_2PbI_2Cl_2$ has a standard single-layer ($n = 1$) RP structure.

We then tested the environmental and thermal stability of $Cs_2PbI_2Cl_2$, issues that strongly impede the application of perovskite materials in solar cells and light-emitting devices. Figure 2a shows the powder XRD pattern of $Cs_2PbI_2Cl_2$ after a 4 month storage in ambient air (~25 °C and ~65 RH%), where no sign of degradation or new phase is observed.

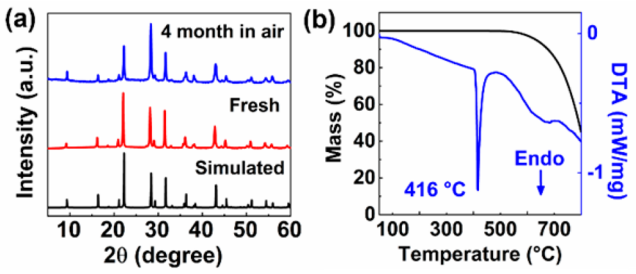

Figure 2. (a) Powder XRD pattern of $Cs_2PbI_2Cl_2$ after a 4 month storage in air (T = ~25 °C and RH = ~65%). (b) TGA and DTA measurements of $Cs_2PbI_2Cl_2$.

Thermal gravimetric analysis (TGA) results show that the sample starts to lose weight at a high temperature of ~520 °C, while the sharp endothermal peak observed in differential thermal analysis (DTA) indicates a congruent melting of $Cs_2PbI_2Cl_2$ at 416 °C. It needs to be mentioned that a second phase with a small exothermal peak at 359 °C appeared at the first cooling process and melted incongruently in the second test cycle, as shown in Figure S4, which could most likely to be $CsPbI_3$ according to the new absorption edge at 1.73 eV in the UV–vis spectrum after the DTA measurements (Figure S5), further confirming the thermodynamic stability of "113" secondary phase and the importance of slow cooling for single crystal growth.

After understanding the melting/crystallization behavior, we used the vertical Bridgman method[21,22] to separate $Cs_2PbI_2Cl_2$ from impurities through slow crystallization and obtained large single crystals of several-millimeter size. These samples of $Cs_2PbI_2Cl_2$ were used for further characterizations of optical and electrical properties. To investigate the relative thermodynamic stability of all the possible mixed halide Cs_2PbX_4 candidates, we performed density functional theory (DFT) calculations. Considering two crystallographic positions for halogens, there are 9 possible compounds in 3 types (schematic view in Figure 3): Cs_2PbX_4 with single halogen

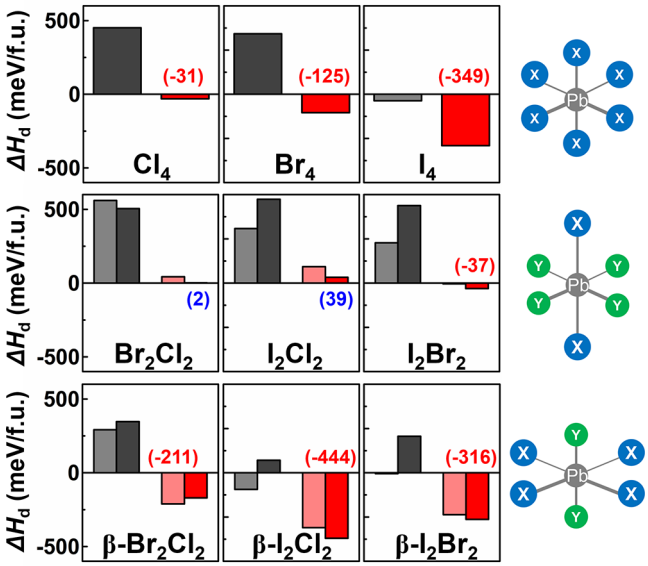

Figure 3. Calculated ΔH_d values of nine possible RP phase lead halide perovskites through different decomposition pathways. The gray and red bars indicate pathways A and B, respectively. Particularly, the light and dark color in mixed halogen cases represent the consideration of halogen exchange (light gray: eq A-1, dark gray: eq A-2; light red: eq B-1, dark red: eq B-2). In parentheses are the least ΔH_d values.

source; $Cs_2PbX_2Y_2$ ($X \neq Y$, $r_X > r_Y$) with elongated octahedron unit (smaller Y in plane); β-$Cs_2PbX_2Y_2$ ($X \neq Y$, $r_X > r_Y$) with compressed octahedron unit (larger X in plane). Decomposition enthalpies (ΔH_d) that appropriately account for the thermodynamic stability of compounds were calculated through different decomposition pathways.[23–25] Basically, there are two kinds of secondary phases: one has two binary compounds of cesium and lead halide salts (eq A), and the other involves two ternary compounds of "113" and "416" phases (eq B). For the mixed halide cases, the interchange of different halogens is as follows:

DOI: 10.1021/jacs.8b06046
J. Am. Chem. Soc. 2018, 140, 11085–11090

$$Cs_2PbX_4 \rightarrow 2CsX + PbX_2 \quad (A)$$

$$Cs_2PbX_2Y_2 \rightarrow 2CsY + PbX_2 \quad (A\text{-}1)$$

$$Cs_2PbX_2Y_2 \rightarrow 2CsX + PbY_2 \quad (A\text{-}2)$$

$$Cs_2PbX_4 \rightarrow 2/3CsPbX_3 + 1/3Cs_4PbX_6 \quad (B)$$

$$Cs_2PbX_2Y_2 \rightarrow 2/3CsPbY_3 + 1/3Cs_4PbX_6 \quad (B\text{-}1)$$

$$Cs_2PbX_2Y_2 \rightarrow 2/3CsPbX_3 + 1/3Cs_4PbY_6 \quad (B\text{-}2)$$

Among all the structures, only $Cs_2PbBr_2Cl_2$ and $Cs_2PbI_2Cl_2$ show positive ΔH_d for all the decomposition pathways, reflecting their thermodynamically stable nature. For the other seven compounds, however, the ΔH_d values through pathway B are negative, indicating tendency for spontaneous decomposition of forming "113" and "416" secondary phases, which agrees with the experimental results perfectly. Though for $Cs_2PbBr_2Cl_2$, a positive ΔH_d is calculated; this is the least positive value of only +2 meV/f.u. Once we consider the realistic situation of forming solid solutions ($CsPbBr_{3-x}Cl_x$, $Cs_4PbBr_{6-x}Cl_x$), it will increase the entropy and further stabilize these reaction products, leading to the decomposition of $Cs_2PbBr_2Cl_2$. Thus, $Cs_2PbI_2Cl_2$ is theoretically the most stable n = 1 RP phase lead halide perovskite in agreement with experiment.

Figure 4a shows that $Cs_2PbI_2Cl_2$ has a sharp optical absorption edge at 3.04 eV. The small kink feature in the absorption edge is attributed to an excitonic absorption.[11] Unlike the strong exciton peak typically observed in 2D hybrid perovskites, the exciton peak of $Cs_2PbI_2Cl_2$ seems to be weaker and could be associated with a reduced excitonic contribution.[11,13] Although the short interlayer spacing is achieved by the Cs^+ (separation distance ~3.10 Å), it is the all-inorganic nature that greatly restrains the dielectric confinement due to the reduced dielectric mismatch between inorganic well and inorganic barrier compared to the long-chain organic barriers.[26] This dielectric mismatch is believed to predominantly enhance the effective Coulomb interaction between electron and hole in the lead halide framework and increase the exciton binding energies of the 2D hybrid perovskites, therefore the reduced dielectric mismatch in $Cs_2PbI_2Cl_2$ could result in the decrease of excitonic features at room temperature.[27−29]

$Cs_2PbI_2Cl_2$ exhibits a photoluminescence (PL) peak at 3.01 eV, close to the excitonic absorption peak. Temperature-dependent PL spectra show that a broad PL emission peak emerged near the lower-energy tail as temperature decreased, while the original PL peak at room temperature was much less altered (Figure S6). Since we did not observe any phase transition down to 100 K, this broad PL peak could most likely be correlated with self-trapping excitons.[16,30,31] The PL emission and time-resolved PL spectra were also recorded and showed in Figure S6, where an average lifetime of ~3.7 ns was observed.

Using a hybrid functional with spin−orbit coupling (HSE + SOC), our calculations predict a direct bandgap for $Cs_2PbI_2Cl_2$, close to the experimental value (Figure 4b).[32,33] The conduction band minimum (CBM) and valence band maximum (VBM) both locate at the M point (1/2, 1/2, 0). The states near the CBM are mainly contributed by Pb 6p states, while those near the VBM are contributed by I 5p/Cl 3p-Pb 6s antibonding states, which is similar to 2D $MA_2Pb(SCN)_2I_2$ and 3D $CsPbCl_3$ and $CsPbI_3$.[34−36]

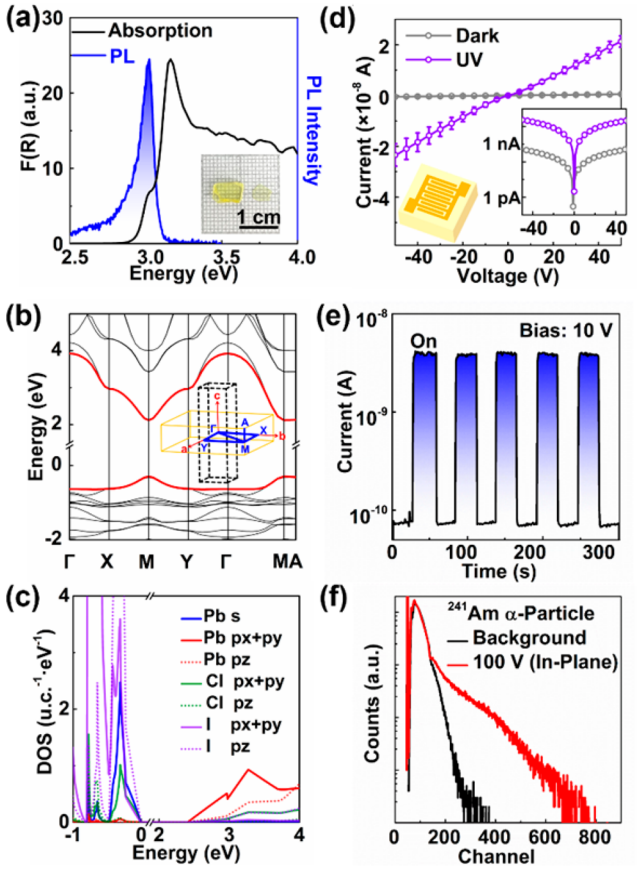

Figure 4. (a) UV−vis absorption and PL spectra of polycrystalline $Cs_2PbI_2Cl_2$ samples. Inset: image of a single crystal obtained by the Bridgman method and a mechanically exfoliated crystal slice. (b) HSE + SOC calculated electronic band structure along the Γ (0, 0, 0)-X(0, 1/2, 0)-M(1/2, 1/2, 0)-Y(1/2, 0, 0)-Γ(0, 0, 0)-M(1/2, 1/2, 0)-A(1/2, 1/2, 1/2) path throughout the Brillouin zone as schemed in the inset and (c) calculated partial DOS of $Cs_2PbI_2Cl_2$. (d) Current−voltage curve of $Cs_2PbI_2Cl_2$ single crystal under 0.6 mW/cm^2 UV light (365 nm) and (e) on−off switching measurements under 10 V bias voltage. Insets in (d) display the interdigitated Au electrode pattern and the logarithmic coordinate I/V chart that shows the symmetric character of current output. (f) ^{241}Am α-particle (E_k = 5.49 MeV) counting response of $Cs_2PbI_2Cl_2$ single crystal under 100 V bias voltage using in-plane electrode configuration.

The highly dispersive bands near the valence and conduction edges for the 3D halide perovskites are credited for their amazing carrier transport properties.[37] The electronic bands of $Cs_2PbI_2Cl_2$ have similarly broad bandwidths near the VBM and CBM. By applying the parabolic band approximation, our DFT calculations predict relatively small electron and hole effective masses for $Cs_2PbI_2Cl_2$ along the $[PbI_2Cl_2]_n^{2n-}$ plane (Table 1). While the hole effective mass is larger, the electron effective mass is comparable to those of

Table 1. Calculated Effective Masses of Electron and Hole of $Cs_2PbI_2Cl_2$, $CsPbCl_3$, and $CH_3NH_3PbI_3$

		m_e^*/m_0	m_h^*/m_0
$Cs_2PbI_2Cl_2$	in-plane	0.237	0.531
	out-of-plane	19.254	7.511
$CsPbCl_3$[38]		0.28	0.18
$CH_3NH_3PbI_3$[37]		0.25	0.19

DOI: 10.1021/jacs.8b06046
J. Am. Chem. Soc. 2018, 140, 11085−11090

$CsPbCl_3$ and $CH_3NH_3PbI_3$. In contrast, along the *c*-axis, perpendicular to the layers, the band dispersions are nearly flat as can be seen between M and A point in reciprocal space (Figure 4b), predicting large effective masses and strong confinement of electrons and holes in the layers, predicting an anisotropic carrier transport property.

The case where the I and Cl ions positions are switched in the structure (i.e., the hypothetical β-$Cs_2PbI_2Cl_2$ where the bridging halides in the plane are I ions and the terminal atoms out of plane are Cl ions) was also considered in order to assess the relative stabilities between the two forms. The calculated density of states (DOS) provides a useful perspective into understanding the destabilization effect of halogen swapping in $Cs_2PbI_2Cl_2$. Because the total energy of a compound is determined by the highest occupied states, we can focus on the band composition near VBM that associates with the antibonding states of I 5p-Pb 6s and Cl 3p-Pb 6s. Since the energy of I 5p orbitals is higher than that of Cl 3p, the antibonding states of I 5p-Pb 6s exhibit higher orbital energy, and the degree of antibonding between Pb 6s and I 5p determines the total energy relation of $Cs_2PbI_2Cl_2$ and β-$Cs_2PbI_2Cl_2$. As a result, the β-$Cs_2PbI_2Cl_2$ form has a narrower bandgap (Figure S7a and c) and higher total energy (−26.282 eV/f.u.) than the $Cs_2PbI_2Cl_2$ (−26.765 eV/f.u.).

We performed UV light measurements to test the photoresponse of $Cs_2PbI_2Cl_2$ using single crystals with (00*l*) orientation of the cleavage facet (Figure S8). As shown in Figure 4d, the compound exhibits a large dark in-plane resistivity of 3.1×10^{11} Ω cm, suggesting a very low intrinsic carrier density. When 0.6 mW/cm^2 UV light (365 nm) illumination was applied, the resistivity markedly decreased by nearly 2 orders of magnitude to 7.5×10^9 Ω cm. Figure 4e shows the reversible on−off switching properties (on−off ratio of ∼60) measured under 10 V bias voltage. The on−off cycling results at low frequencies in Figure S10 showed a highly stable and reproducible behavior, and a rising time of ∼0.2 s and a decay time of ∼0.06 s for the UV-light detector could be extracted (Figure S11).

Because of the relatively high density and high atomic number elements in this material, the $CsPbI_2Cl_2$ has potential as a hard radiation detector.[39−42] We therefore made an initial assessment using an ^{241}Am α-particle source. The α-particle detection of $Cs_2PbI_2Cl_2$ device was operated using pulse mode, where the generated pulses of α-particle were collected separately in a given time period. Under the ^{241}Am α-particle source (E_k = 5.49 MeV), $Cs_2PbI_2Cl_2$ single crystal with in-plane electrode configuration showed a clear counting signal under 100 V bias voltage (Figure 4f). The demonstration of response to UV light and α-particles suggests that $Cs_2PbI_2Cl_2$ can be further developed as a promising wide-gap semiconductor for radiation detection at room temperature.

The chemical investigation of the all-inorganic RP phase mixed halide perovskites was also expanded to the mixed Pb/Sn systems. The Sn-based analogue, $Cs_2SnI_2Cl_2$, can be synthesized according to our recent results.[43] Compared to $Cs_2PbI_2Cl_2$, $Cs_2SnI_2Cl_2$ has a thinner but longer unit cell (smaller *a*/*b* and larger *c*, Table S10). As shown in Figure 5, the lattice parameters change linearly for the $Cs_2Pb_xSn_{1-x}I_2Cl_2$ solid solutions, but the band gaps show an anomalous bowing evolution. When Sn is introduced, the band gaps quickly drop to ∼2.52 eV for the intermediate compositions (x = 0.25, 0.5, 0.75) and increase again as reaching the pure Sn analogue (2.6 eV). This bowing evolution of band gap is also observed in 3D

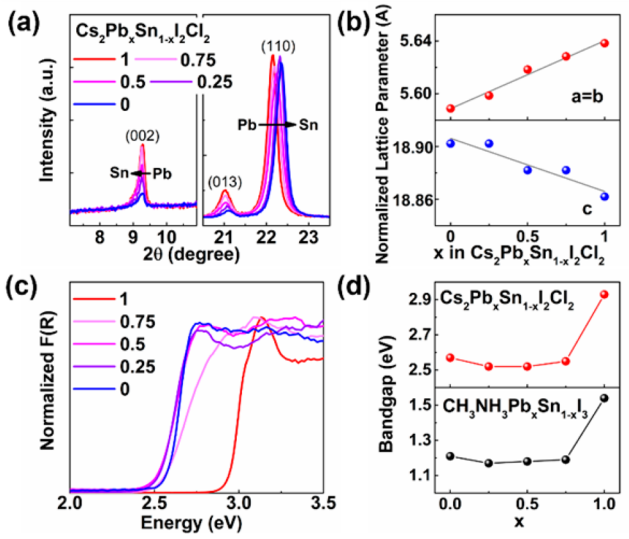

Figure 5. (a) Powder XRD, (b) lattice parameters, (c) UV−vis absorption spectra, and (d) band gap evolution of $Cs_2Pb_{1-x}Sn_xI_2Cl_2$ solid solutions. Similar anomalous evolution of band gaps observed in $CH_3NH_3Pb_{1-x}Sn_xI_3$ solid solution is also drawn for comparison in (d).[44]

$CH_3NH_3Pb_{1-x}Sn_xI_3$ solid solutions and was attributed to the competition between the spin−orbit coupling (SOC) and the lattice distortion.[44,45] In the $Cs_2Pb_{1-x}Sn_xI_2Cl_2$ case, however, no octahedral distortion is observed and the bowing effect could be related to the anomalous decrease of lattice parameter *c*, which needs further investigation.

The size of A-cations is also found to play an important role for stabilizing the RP structure. When Rb^+ was used instead of Cs^+, the RP structure collapsed, and $RbPbI_3$ and Rb_3PbCl_5 dominated as main products (Figure S13). In addition, no sign for the existence of high-member RP phases could be distinguished in the nominal compositions of either $Cs_{n+1}Pb_nI_{n+1}Cl_{2n}$ (Cs^+ as both spacer and interlayer cations) or $Cs_2Rb_{n-1}Pb_nI_{n+1}Cl_{2n}$ (Cs^+ as spacer, Rb^+ as interlayer cations). All of these results emphasize the uniqueness of $Cs_2PbI_2Cl_2$.

CONCLUSION

In conclusion, $Cs_2PbI_2Cl_2$ is an all-inorganic 2D RP phase perovskite with ordered mixed halides. The compound exhibits a direct band gap of 3.04 eV and a large in-plane resistivity of $>10^{11}$ Ω cm. A combined DFT and experimental study excludes all other candidates in the Cs_2PbX_4 (X = Cl, Br, I) system which decompose through an energetically favored pathway involving the two ternary compounds $CsPbX_3$ and Cs_4PbX_6. A strong UV-light response and an effective in-plane α-particle counting ability confirm the very promising optoelectronic properties of 2D $Cs_2PbI_2Cl_2$. The finding of $Cs_2PbI_2Cl_2$ expands the low-dimensional halide perovskite family and opens new opportunities for functionality beyond photovoltaics.

ASSOCIATED CONTENT

Supporting Information

The Supporting Information is available free of charge on the ACS Publications website at DOI: 10.1021/jacs.8b06046.

Experimental details and theoretical calculation methods, crystallographic data of $Cs_2PbI_2Cl_2$, detailed

DOI: 10.1021/jacs.8b06046
J. Am. Chem. Soc. 2018, 140, 11085−11090

calculation data, additional XRD, UV−vis absorption, temperature-dependent PL spectra, photo- and α-particle-response measurements, characterization of $Cs_2Sn_xPb_{1-x}I_2Cl_2$ solid solution (PDF)
Crystallographic file of $Cs_2PbI_2Cl_2$ (CIF)

AUTHOR INFORMATION

Corresponding Authors

*dong913@mail.tsinghua.edu.cn
*m-kanatzidis@northwestern.edu

ORCID

Jiangwei Li: 0000-0002-4089-1747
Yihui He: 0000-0002-1057-6826
Constantinos C. Stoumpos: 0000-0001-8396-9578
Guangda Niu: 0000-0002-9285-4147
Hang Guo: 0000-0001-7004-1527
Dong Wang: 0000-0002-0594-0515
Mercouri G. Kanatzidis: 0000-0003-2037-4168

Author Contributions

‖These authors contributed equally to this work.

Notes

The authors declare no competing financial interest.

ACKNOWLEDGMENTS

This work was primarily supported by the Department of Energy, Office of Science, Basic Energy Sciences, under Grant SC0012541 (synthesis, XRD, and physical characterization). Support from the National Natural Science Foundation of China under grant no. 91433205 (photoresponse characterizations) and no. 21673123 and the Ministry of Science and Technology of China under grant no. 2015CB655002 (DFT calculations) are also acknowledged. Computational resources were provided by the National Supercomputer Center in Guangzhou. J. L. gratefully acknowledges financial support from the Joint Educational Ph.D. Program of Chinese Scholarship Council (CSC).

REFERENCES

(1) Ruddlesden, S.; Popper, P. *Acta Crystallogr.* **1957**, *10* (8), 538−539.
(2) Battle, P.; Blundell, S.; Green, M.; Hayes, W.; Honold, M.; Klehe, A.; Laskey, N.; Millburn, J.; Murphy, L.; Rosseinsky, M.; et al. *J. Phys.: Condens. Matter* **1996**, *8* (32), L427.
(3) Tarascon, J.-M.; Greene, L.; McKinnon, W.; Hull, G.; Geballe, T. *Science* **1987**, *235* (4794), 1373−1376.
(4) Lee, C.-H.; Orloff, N. D.; Birol, T.; Zhu, Y.; Goian, V.; Rocas, E.; Haislmaier, R.; Vlahos, E.; Mundy, J. A.; Kourkoutis, L. F.; et al. *Nature* **2013**, *502* (7472), 532.
(5) Khalifah, P.; Osborn, R.; Huang, Q.; Zandbergen, H.; Jin, R.; Liu, Y.; Mandrus, D.; Cava, R. *Science* **2002**, *297* (5590), 2237−2240.
(6) Seitz, L. C.; Dickens, C. F.; Nishio, K.; Hikita, Y.; Montoya, J.; Doyle, A.; Kirk, C.; Vojvodic, A.; Hwang, H. Y.; Norskov, J. K. *Science* **2016**, *353* (6303), 1011−1014.
(7) Tsai, H.; Nie, W.; Blancon, J.-C.; Stoumpos, C. C.; Asadpour, R.; Harutyunyan, B.; Neukirch, A. J.; Verduzco, R.; Crochet, J. J.; Tretiak, S.; et al. *Nature* **2016**, *536* (7616), 312.
(8) Yuan, M.; Quan, L. N.; Comin, R.; Walters, G.; Sabatini, R.; Voznyy, O.; Hoogland, S.; Zhao, Y.; Beauregard, E. M.; Kanjanaboos, P.; et al. *Nat. Nanotechnol.* **2016**, *11* (10), 872.
(9) Smith, I. C.; Hoke, E. T.; Solis-Ibarra, D.; McGehee, M. D.; Karunadasa, H. I. *Angew. Chem.* **2014**, *126* (42), 11414−11417.
(10) Cao, D. H.; Stoumpos, C. C.; Farha, O. K.; Hupp, J. T.; Kanatzidis, M. G. *J. Am. Chem. Soc.* **2015**, *137* (24), 7843−7850.
(11) Stoumpos, C. C.; Cao, D. H.; Clark, D. J.; Young, J.; Rondinelli, J. M.; Jang, J. I.; Hupp, J. T.; Kanatzidis, M. G. *Chem. Mater.* **2016**, *28* (8), 2852−2867.
(12) Cao, D. H.; Stoumpos, C. C.; Yokoyama, T.; Logsdon, J. L.; Song, T.-B.; Farha, O. K.; Wasielewski, M. R.; Hupp, J. T.; Kanatzidis, M. G. *ACS Energy Lett.* **2017**, *2* (5), 982−990.
(13) Stoumpos, C. C.; Soe, C. M. M.; Tsai, H.; Nie, W.; Blancon, J.-C.; Cao, D. H.; Liu, F.; Traoré, B.; Katan, C.; Even, J.; Mohite, A. D.; Kanatzidis, M. G. *Chem.* **2017**, *2* (3), 427−440.
(14) Kawano, N.; Koshimizu, M.; Sun, Y.; Yahaba, N.; Fujimoto, Y.; Yanagida, T.; Asai, K. *J. Phys. Chem. C* **2014**, *118* (17), 9101−9106.
(15) Knutson, J. L.; Martin, J. D.; Mitzi, D. B. *Inorg. Chem.* **2005**, *44* (13), 4699−4705.
(16) Nazarenko, O.; Kotyrba, M. R.; Wörle, M.; Cuervo-Reyes, E.; Yakunin, S.; Kovalenko, M. V. *Inorg. Chem.* **2017**, *56* (19), 11552−11564.
(17) Grote, C.; Ehrlich, B.; Berger, R. F. *Phys. Rev. B: Condens. Matter Mater. Phys.* **2014**, *90* (20), 205202.
(18) Xiao, Z.; Meng, W.; Wang, J.; Mitzi, D. B.; Yan, Y. *Mater. Horiz.* **2017**, *4* (2), 206−216.
(19) Yu, Y.; Zhang, D.; Yang, P. *Nano Lett.* **2017**, *17* (9), 5489−5494.
(20) Song, J.; Xu, L.; Li, J.; Xue, J.; Dong, Y.; Li, X.; Zeng, H. *Adv. Mater.* **2016**, *28* (24), 4861−4869.
(21) Stoumpos, C. C.; Malliakas, C. D.; Peters, J. A.; Liu, Z.; Sebastian, M.; Im, J.; Chasapis, T. C.; Wibowo, A. C.; Chung, D. Y.; Freeman, A. J.; et al. *Cryst. Growth Des.* **2013**, *13* (7), 2722−2727.
(22) Lin, W.; Stoumpos, C. C.; Liu, Z.; Das, S.; Kontsevoi, O. Y.; He, Y.; Malliakas, C. D.; Chen, H.; Wessels, B. W.; Kanatzidis, M. G. *ACS Photonics* **2017**, *4* (7), 1805−1813.
(23) Perdew, J. P.; Burke, K.; Ernzerhof, M. *Phys. Rev. Lett.* **1996**, *77* (18), 3865.
(24) Xiao, Z.; Du, K.-Z.; Meng, W.; Wang, J.; Mitzi, D. B.; Yan, Y. *J. Am. Chem. Soc.* **2017**, *139* (17), 6054−6057.
(25) Xiao, Z.; Du, K.-Z.; Meng, W.; Mitzi, D.; Yan, Y. *Angew. Chem., Int. Ed.* **2017**, *56* (40), 12107.
(26) Sapori, D.; Kepenekian, M.; Pedesseau, L.; Katan, C.; Even, J. *Nanoscale* **2016**, *8* (12), 6369−6378.
(27) Ishihara, T.; Takahashi, J.; Goto, T. *Phys. Rev. B: Condens. Matter Mater. Phys.* **1990**, *42* (17), 11099−11107.
(28) Hong, X.; Ishihara, T.; Nurmikko, A. *Phys. Rev. B: Condens. Matter Mater. Phys.* **1992**, *45* (12), 6961.
(29) Tanaka, K.; Takahashi, T.; Kondo, T.; Umebayashi, T.; Asai, K.; Ema, K. *Phys. Rev. B: Condens. Matter Mater. Phys.* **2005**, *71* (4), 045312.
(30) Gauthron, K.; Lauret, J.; Doyennette, L.; Lanty, G.; Al Choueiry, A.; Zhang, S.; Brehier, A.; Largeau, L.; Mauguin, O.; Bloch, J. *Opt. Express* **2010**, *18* (6), 5912−5919.
(31) Yangui, A.; Garrot, D.; Lauret, J.-S.; Lusson, A.; Bouchez, G.; Deleporte, E.; Pillet, S.; Bendeif, E.-E.; Castro, M.; Triki, S.; et al. *J. Phys. Chem. C* **2015**, *119* (41), 23638−23647.
(32) Kresse, G.; Furthmüller, J. *Phys. Rev. B: Condens. Matter Mater. Phys.* **1996**, *54* (16), 11169.
(33) Kresse, G.; Furthmüller, J. *Comput. Mater. Sci.* **1996**, *6* (1), 15−50.
(34) Xiao, Z.; Meng, W.; Saparov, B.; Duan, H.-S.; Wang, C.; Feng, C.; Liao, W.; Ke, W.; Zhao, D.; Wang, J.; et al. *J. Phys. Chem. Lett.* **2016**, *7* (7), 1213−1218.
(35) Ghebouli, M.; Ghebouli, B.; Fatmi, M. *Phys. B* **2011**, *406* (9), 1837−1843.
(36) Giorgi, G.; Fujisawa, J.-I.; Segawa, H.; Yamashita, K. *J. Phys. Chem. C* **2014**, *118* (23), 12176−12183.
(37) Umari, P.; Mosconi, E.; De Angelis, F. *Sci. Rep.* **2015**, *4*, 4467.
(38) Qian, J.; Xu, B.; Tian, W. *Org. Electron.* **2016**, *37*, 61−73.
(39) Androulakis, J.; Peter, S. C.; et al. *Adv. Mater.* **2011**, *23* (36), 4163−4167.
(40) Johnsen, S.; Liu, Z.; Peters, J. A.; Song, J.-H.; Nguyen, S.; Malliakas, C. D.; Jin, H.; Freeman, A. J.; Wessels, B. W.; Kanatzidis, M. G. *J. Am. Chem. Soc.* **2011**, *133* (26), 10030−10033.

DOI: 10.1021/jacs.8b06046
J. Am. Chem. Soc. 2018, 140, 11085−11090

(41) He, Y.; Kontsevoi, O. Y.; Stoumpos, C. C.; Trimarchi, G. G.; Islam, S. M.; Liu, Z.; Kostina, S. S.; Das, S.; Kim, J.-I.; Lin, W.; Wessels, B. W.; Kanatzidis, M. G. *J. Am. Chem. Soc.* **2017**, *139* (23), 7939−7951.
(42) He, Y.; Matei, L.; Jung, H. J.; McCall, K. M.; Chen, M.; Stoumpos, C. C.; Liu, Z.; Peters, J. A.; Chung, D. Y.; Wessels, B. W.; Wasielewski, M. R.; Dravid, V. P.; Burger, A.; Kanatzidis, M. G. *Nat. Commun.* **2018**, *9* (1), 1609.
(43) Li, J.; Stoumpos, C. C.; Trimarchi, G. G.; Chung, I.; Mao, L.; Chen, M.; Wasielewski, M. R.; Wang, L.; Kanatzidis, M. G. *Chem. Mater.* **2018**, *30*, 4847−4856.
(44) Im, J.; Stoumpos, C. C.; Jin, H.; Freeman, A. J.; Kanatzidis, M. G. *J. Phys. Chem. Lett.* **2015**, *6* (17), 3503−3509.
(45) Hao, F.; Stoumpos, C. C.; Chang, R. P.; Kanatzidis, M. G. *J. Am. Chem. Soc.* **2014**, *136* (22), 8094−8099.

DOI: 10.1021/jacs.8b06046
J. Am. Chem. Soc. 2018, 140, 11085−11090